

Positron-annihilation study of the half-metallic ferromagnet NiMnSb: Experiment

K. E. H. M. Hanssen,* P. E. Mijnaerends, and L. P. L. M. Rabou
Netherlands Energy Research Foundation ECN, 1755 ZG Petten, The Netherlands

K. H. J. Buschow
Philips Research Laboratories, 5600 JA Eindhoven, The Netherlands
 (Received 29 December 1989)

Spin-polarized measurements of the two-dimensional angular correlation of annihilation radiation in NiMnSb are presented. By making use of the inherent partial polarization of the positron beam and the alignment of the magnetic domains with the aid of an external magnetic field, the sum and difference of the spin-dependent contributions to the angular correlation have been obtained for integration directions $\langle 100 \rangle$, $\langle 110 \rangle$, and $\langle 111 \rangle$. The results are compared with calculated distributions. A least-squares analysis of the data yields a value of $(-8.4 \pm 0.1) \times 10^{-3}$ for the three-photon difference effect in NiMnSb and establishes the half-metallic character of the band structure with an accuracy of $\sim \pm_{-0.02}^{+0.01}$ electrons per formula unit.

I. INTRODUCTION

Half-metallic ferromagnets have raised considerable interest in recent years. Band-structure calculations for these materials yield a surprising result: the band structure for one spin direction is metallic, while that for the opposite spin direction has a gap straddling the Fermi level, a situation typical of a semiconductor.¹⁻⁶ The $C1_b$ Heusler compound NiMnSb is a prototype of this class of systems. This paper describes an investigation of the electronic structure of NiMnSb by a measurement of the two-dimensional angular correlation of annihilation radiation (2D-ACAR) $N(p_y, p_z)$,

$$N(p_y, p_z) = C \int \rho(\mathbf{p}) dp_x. \quad (1)$$

Here $\rho(\mathbf{p})$ is the two-photon momentum density, \mathbf{p} is the total momentum of the annihilation quanta, and C is a geometry-dependent constant. Spin-polarized results have been obtained by making use of the inherent polarization of the positron beam. A comparison of these experimental data with the calculated momentum density of annihilation photon pairs provides information on the electronic structure, in particular on the geometry of the Fermi surface.

There is limited experimental information pertaining to the electronic structure of ferromagnetic materials such as NiMnSb,⁷⁻¹² PtMnSb,^{7,8,11,13} CoMnSb,¹¹ CrO₂,¹⁴ and NiUSn,¹⁵ which are all predicted to be half-metallic. Although many of the results found are not inconsistent with the band structures calculated for these materials, these experimental studies do not give direct evidence for the existence or nonexistence of half-metallic magnetism. The data on NiMnSb, for instance, are mainly of optical origin.^{7,8} However, the presence of the surface causes segregation in NiMnSb,⁹ leading to Sb enrichment of the surface. Hence surface-sensitive techniques may not be adequate to test the half-metallic nature of NiMnSb. For a 2D-ACAR experiment, on the other hand, segregation

in the outermost layers of the sample is unimportant as the average implantation depth of the positrons¹⁶ ($\sim 40 \mu\text{m}$) is sufficiently large to guarantee annihilation with electrons in the bulk. This fact, together with the possibility of performing spin-polarized measurements, makes the angular correlation technique ideally suited to test the half-metallic properties of NiMnSb.

The outline of this paper is as follows. The theory of polarized-positron annihilation is briefly discussed in Sec. II. It is shown how, after proper normalization of the measured spin-polarized 2D-ACAR distributions, the comparison between experiment and theory can be cast in the form of a one-parameter least-squares fit. Section III describes the sample preparation, while the experimental results are presented in Sec. IV. These results are compared with theoretical distributions, calculated by Hanssen and Mijnaerends¹⁷ on the basis of the Korringa-Kohn-Rostoker (KKR) method. Section V addresses the key question of this paper, namely the half-metallic character of the band structure of NiMnSb. A rigid-band approach is adopted and the Stoner splitting between the two spin bands is varied, causing a transfer of electrons from one electron-spin population to the other. The spin-dependent momentum distributions are calculated for varying amounts of electron transfer and compared to the experimental data, thus allowing us to draw conclusions concerning the position of the Fermi level with respect to the two spin bands, and hence about the half-metallic character of the compound.

II. POLARIZED-POSITRON ANNIHILATION

In polarized-positron annihilation experiments¹⁸ use is made of the fact that the positron beam emitted by a radioactive source possesses an average polarization P along the axis of the beam as a result of nonconservation of parity in β decay. The source used in this experiment is a ²²Na line source¹⁹ with $P \approx 0.3$.²⁰ Two-photon annihilation only takes place between a positron (e^+) and an

electron with opposite spin. Consequently, an electron-spin polarization opposite to P results in preferential annihilation of the majority-spin electrons. Measurements of the angular correlation $N_{\uparrow(\downarrow)}(p_y, p_z)$ when the electrons are spin aligned by a magnetic field parallel (\uparrow) or antiparallel (\downarrow) to the e^+ polarization yield, after subtraction, a magnetic difference distribution²⁰ (for a derivation see the Appendix)

$$\begin{aligned} \Delta N(p_y, p_z) &\equiv N_{\uparrow}(p_y, p_z) - N_{\downarrow}(p_y, p_z) \\ &= P \left[\frac{\rho_+(p_y, p_z)}{\rho_+} - \frac{\rho_-(p_y, p_z)}{\rho_-} + O(10^{-4}) \right] \end{aligned} \quad (2)$$

and a magnetic sum distribution

$$\begin{aligned} \sum N(p_y, p_z) &\equiv N_{\uparrow}(p_y, p_z) + N_{\downarrow}(p_y, p_z) \\ &= \frac{\rho_+(p_y, p_z)}{\rho_+} + \frac{\rho_-(p_y, p_z)}{\rho_-} + O(10^{-4}). \end{aligned} \quad (3)$$

The two expressions can be combined to give¹⁸

$$\begin{aligned} -\Delta N(p_y, p_z) + C \sum N(p_y, p_z) \\ = \frac{2C}{\rho_- - \rho_+} [\rho_-(p_y, p_z) - \rho_+(p_y, p_z)]. \end{aligned} \quad (4)$$

Here $\rho_\sigma(p_y, p_z) \equiv \int \rho_\sigma(\mathbf{p}) dp_x$ and $\rho_\sigma \equiv \int \rho_\sigma(\mathbf{p}) d\mathbf{p}$ are integrals of the computed majority-spin (+) and minority-spin (-) momentum densities, while

$$C = P \frac{\rho_- - \rho_+}{\rho_- + \rho_+}. \quad (5)$$

When Eq. (4) is used to compare the measured distributions $N_{\uparrow(\downarrow)}(p_y, p_z)$ with calculated (once-integrated) densities $\rho_\sigma(p_y, p_z)$ there is only one fit parameter, C , which may be determined by a least-squares analysis.²¹ In the Appendix it is shown that, apart from a geometry-dependent factor, C equals to a good approximation the three-photon difference effect $P^{3\gamma}$ defined by¹⁸

$$P^{3\gamma} \equiv \frac{N_{\downarrow}^{3\gamma} - N_{\uparrow}^{3\gamma}}{N_{\downarrow}^{3\gamma} + N_{\uparrow}^{3\gamma}}, \quad (6)$$

where $N_{\uparrow(\downarrow)}^{3\gamma}$ is the field-dependent rate of 3γ events. Equations (2)–(4) are equally applicable when the experimental and theoretical momentum distributions $N_{\uparrow(\downarrow)}(p_y, p_z)$ and $\rho_\sigma(p_y, p_z)$ are replaced by their ‘‘Lock-Crisp-West (LCW)-folded’’ counterparts, $F_{\uparrow(\downarrow)}(p_y, p_z)$ and $h_\sigma(p_y, p_z)$, respectively, obtained by a mapping of the original distributions onto \mathbf{k} space^{22,23} (see below).

As the right-hand side of Eq. (4) contains only the difference of the majority- and minority-spin momentum densities, the core contributions will cancel to a good approximation. This is an advantage because it takes away the need to compute the core contributions which are affected by enhancement due to positron-electron correlation effects.²⁴ The enhancement of the valence-band contributions, which is larger in magnitude but less strongly momentum dependent than the core enhancement, has

TABLE I. Results of the positron-lifetime measurements in NiMnSb.

lifetime (ps)	intensity (%)	assignment
τ_1 162	I_1 79	bulk
τ_2 319	I_2 19	bulk and source
τ_3 1436	I_3 3	source

not been taken into account in the comparison between experiment and theory as it will not significantly affect the structure in the difference distribution.

III. SAMPLE PREPARATION

The NiMnSb single crystal, which was used for all three integration directions, was prepared by means of the Bridgman method starting from a pure alloy obtained by arc melting in an atmosphere of purified Ar gas. The purity of the starting materials was 99.9%. The sample was shaped in the form of a disk of 8 mm diameter. In order to avoid gradients in the γ -ray intensities on the detectors resulting from angle-dependent γ -ray absorption in the sample, the face of the sample turned towards the source is not normal to the positron beam but is bevelled over approximately 4° .

Positrons are incident along the p_z axis which was chosen to coincide with a direction of symmetry in the crystal. For the measurement with integration direction p_x parallel to a $\langle 110 \rangle$ direction and p_z along $\langle 221 \rangle$ the sample was shaped by means of mechanical polishing followed by electropolishing. For the measurements integrated along $\langle 100 \rangle$ and $\langle 111 \rangle$ the sample was reshaped by means of spark erosion in such a way that $p_z = \langle 110 \rangle$ and subsequently electropolished. After each shaping procedure the sample was carefully annealed at 400°C . X-ray diffraction showed a mosaic spread less than 1° . Subsequent positron-annihilation lifetime measurements resulted in a lifetime spectrum with three components (see Table I). τ_3 is a source term, τ_1 is ascribed to annihilation in the bulk, while τ_2 possibly is a mixture of a source term (360 ps, $8 \pm 1\%$) and a second component due to annihilation from a shallow trap at the empty $(\frac{1}{2}, \frac{1}{2}, \frac{1}{2})$ position in the $C1_b$ structure (see Fig. 1 in Ref. 17). There was no indication for the presence of vacancies. Microprobe spot measurements, in which the electron beam penetration was $\sim 1 \mu\text{m}$, and line scans yielded a chemical composition of $\text{Ni}_{1.020}\text{Mn}_{0.984}\text{Sb}_{0.996}$. Measurements on a partly electropolished sample showed no detectable changes in composition due to electropolishing.

IV. RESULTS

The measurements, performed with a 2D-ACAR set-up described in detail elsewhere,^{19,25} yield momentum densities integrated along p_x , the component of \mathbf{p} along the line connecting the detectors. In consecutive measurements the sample was orientated with p_x within 1° of a $\langle 100 \rangle$, $\langle 110 \rangle$, or $\langle 111 \rangle$ direction.

The angular resolution of the experiment consists of a geometrical component and a contribution due to e^+ thermal motion. The latter is given by $0.0306 (m^*T)^{1/2}$ mrad full width at half maximum (FWHM), where m^* is the effective positron mass and T the temperature in K. We have estimated the e^+ contribution by substituting for m^* the positron band mass in NiMnSb, which we calculate at 1.33 times the electron mass m_0 . The resulting width of the resolution is underestimated as also e^+ -electron and e^+ -phonon interactions with accompanying quasiparticle lifetime effects contribute to m^* and thus to the thermal smearing.²⁶ Experimental values for m^*/m_0 in metals and semiconductors²⁷⁻²⁹ lie between 1.2 and 2.3. However, since in our case the e^+ contribution to the resolution is relatively small and adds quadratically to the optical resolution, a greater effective mass will not substantially change the results.

The experiments with integration direction $\langle 110 \rangle$ were performed at $T = 27$ K. After changes to the cooling of the sample the measurements integrated along $\langle 100 \rangle$ and $\langle 111 \rangle$ were performed at 8 K. This resulted in a slightly improved angular resolution (see Table II, fourth column). All distributions have been sampled with a bin size of 0.28×0.28 mrad². For each integration direction we have performed measurements for the 6-T magnetic field parallel and antiparallel to the average positron polarization. The total accumulated numbers of counts in the distributions (for each magnetic field direction) after subtraction of the background are given in Table II. Subsequently, the distributions have been corrected for the experimentally determined momentum sampling function.²³

The theoretical spin-polarized distributions have been calculated earlier by Hanssen and Mijnders^{17,30} using Eqs. (2) and (3). These calculations employ a plane-wave formulation^{31,32} of the KKR method to evaluate the two-photon momentum density and the positron probability distribution in the crystal. From these distributions the magnetic sum and difference distributions have been calculated.

Results for the measured and calculated 2D-ACAR difference distributions are presented in Figs. 1–3 (the rather featureless sum distributions are not shown). To reduce noise the distributions have been smoothed on a 5×5 mesh. In spite of the fact that no use has been made of the crystal symmetry to further reduce the noise in the experimental data, Figs. 1–3 show a detailed agreement between the experimental and theoretical distributions for all three orientations. The fourfold, twofold, and

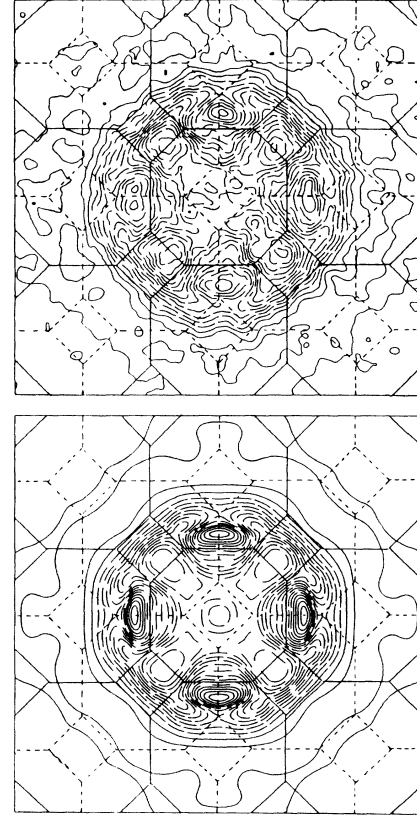


FIG. 1. Difference between the (normalized) 2D-ACAR distributions corresponding to the (once-integrated) momentum densities of the majority- and minority-spin electrons in NiMnSb. The direction of integration is $\langle 100 \rangle$. Superimposed is the projection of the Brillouin zones onto the (p_y, p_z) plane. The zone diameter in the p_y and p_z direction is 1.123 a.u. Solid (dashed) contours denote a positive (negative) density. Top: experiment, bottom: theory.

threefold symmetries corresponding to the respective directions of integration are clearly visible. The agreement is all the more remarkable if one realizes that the difference distribution is at most 3% of either of the measured field-dependent 2D-ACAR distributions.

The momentum distribution $\rho(\mathbf{p})$ is determined by the geometry of the Fermi surface and by the \mathbf{p} dependence of the positron-electron wave-function overlap.¹⁷ The signature of the Fermi surface may be enhanced by application of the LCW theorem.²² This procedure, which also holds in projection, maps $\rho(\mathbf{p})$ onto \mathbf{k} space by folding over reciprocal-lattice vectors.²³ In the ideal case of a

TABLE II. Characteristics of the measurements. The data for the accumulated number of counts (N) per magnetic field direction have been corrected for a background due to accidental coincidences. The angular resolution (Δp) and the angular resolution after interpolation (Δp_i) include broadening due to e^+ thermal motion.

Integration direction	N	T (K)	Δp (mrad ² FWHM)	Δp_i (mrad ² FWHM)
$\langle 100 \rangle$	9×10^7	8	0.55×0.36	0.61×0.59
$\langle 110 \rangle$	8×10^7	27	0.58×0.40	0.62×0.46
$\langle 111 \rangle$	6×10^7	8	0.55×0.36	0.55×0.36

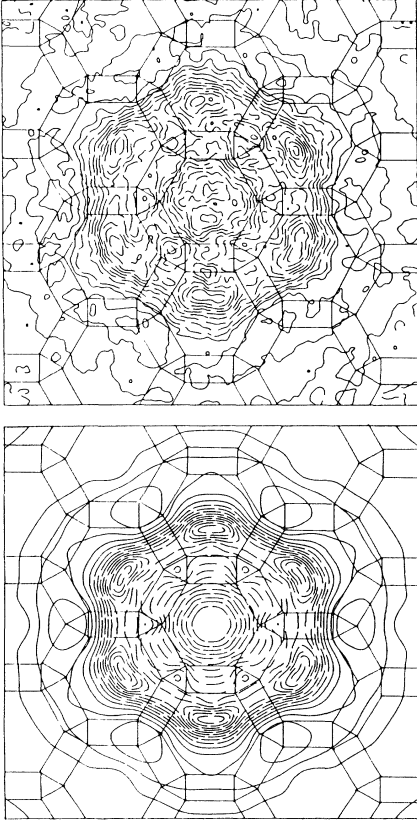


FIG. 2. Same as Fig. 1 for integration direction $\langle 110 \rangle$.

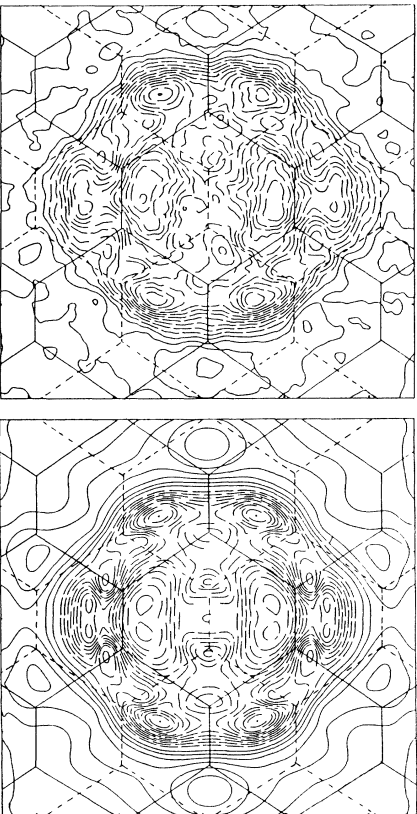


FIG. 3. Same as Fig. 1 for integration direction $\langle 111 \rangle$.

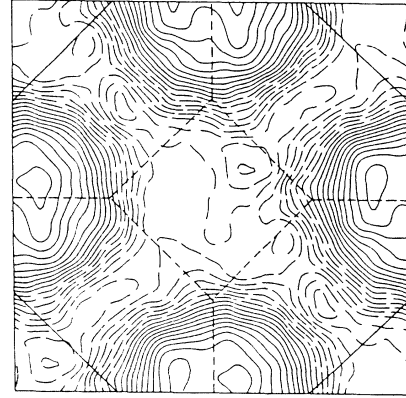


FIG. 4. LCW-folding of the difference between the measured 2D-ACAR distributions in NiMnSb. The direction of integration is $\langle 100 \rangle$. Solid (dashed) contours denote a positive (negative) density.

constant e^+ wave function the LCW-folded distribution consists of a constant contribution from the filled bands with superimposed on it (a projection of) the Fermi surface. For a realistic positron wave function the theorem holds approximately. To facilitate LCW folding of the experimental data it was necessary to interpolate the magnetic sum and difference distributions prior to folding in order to make the sampling mesh commensurate with the reciprocal lattice (lattice constant³³ $a = 11.187$ a.u.). At the same time the coordinate system was rotated to make it coincide with that of the calculated distributions. The broadening effect on the angular resolution caused by the interpolation was estimated by performing the same operations on a positronium peak measured in a quartz single crystal. The widths of the interpolated peaks were obtained by a Gaussian fit. The results of this analysis are given in the fifth column of Table II. Also the LCW-folded distributions were smoothed on a 5×5 mesh. By the combined effect of interpolation and smoothing the resolution deteriorated to approximately 1.0×0.9 mrad² FWHM.

Figures 4–6 show the LCW-folded distributions. The distribution integrated along $\langle 100 \rangle$ in Fig. 4 clearly

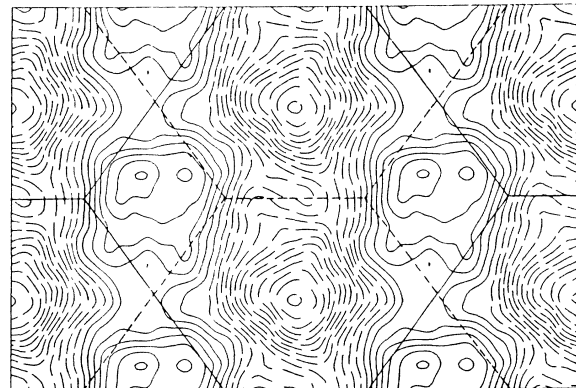


FIG. 5. Same as Fig. 4 for integration direction $\langle 110 \rangle$.

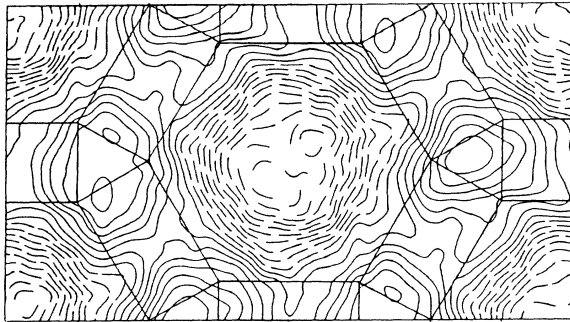


FIG. 6. Same as Fig. 4 for integration direction $\langle 111 \rangle$.

shows the necks of bands 13 and 14 (cf. Fig. 4 in Ref. 17; please note that the Fermi surfaces in that figure are shown in the form of hole sheets). The electron sheets of these two bands form a system of tubes. The $\langle 110 \rangle$ integrated distribution in Fig. 5 reveals the tubes and their crossings. Figure 6 shows the $\langle 111 \rangle$ integrated measurement with its expected threefold symmetry. The structure manifested in this figure is mainly due to the nested bellies of the Fermi-surface hole sheets.

The experimental and theoretical LCW distributions have been compared quantitatively by performing least-squares fits of the calculated LCW distributions to the experimental ones, using Eq. (4) with the constant C as a fitting parameter. In these fits the unsmoothed experimental distributions were used. The theoretical data were convoluted with the experimental resolution (given in the last column of Table II) by means of Hermite-Gauss quadrature. The fits yielded C and hence, through Eq. (A10), the approximate value of $P^{3\gamma}$, the three-photon difference effect. The values of $P^{3\gamma}$ obtained from fits for the three symmetry directions are shown in Table III. Although determined independently, they are equal within the experimental uncertainty and of the same order as those measured by Berko and Mills in Gd and Fe.¹⁸ The quality of the fits, expressed in terms of a reduced χ -squared value, will be discussed in the following section in connection with the question whether NiMnSb is half-metallic or not.

V. DISCUSSION

The key question underlying the present study was whether the electronic band structure of NiMnSb is indeed half-metallic, as predicted by theory. This can be

TABLE III. Results of the least-squares approximation. In addition to the results for $P^{3\gamma}$, the number of degrees of freedom (ν) and the normalized χ -squared values (χ^2/ν) are given.

Integration direction	$10^3 P^{3\gamma}$	ν	χ^2/ν
$\langle 100 \rangle$	-8.4 ± 0.1	495	1.3
$\langle 110 \rangle$	-8.4 ± 0.2	351	1.0
$\langle 111 \rangle$	-8.5 ± 0.1	558	1.5

investigated by studying the quality of the fits for modeled band structures, obtained by slightly raising the Fermi level for one spin population and lowering it for the other while keeping the total number of electrons constant to the nominal number of 22 band electrons per formula unit (f.u.). This is equivalent to transferring a small number of electrons from one spin population to the other by applying a variable Stoner shift. Fractions of 1, 2, 4, and 6×10^{-2} electrons/f.u. were moved either way. Per fraction of 10^{-2} electrons the majority-spin Fermi level had to be raised or lowered by 1 mRy; the corresponding shift in the minority-spin Fermi level was 2-mRy apart from the obvious extra shift to overcome the gap. For all these different band populations the once-integrated momentum density distributions were computed and folded to yield an LCW-folded distribution. The goodness-of-fit parameter χ^2 , obtained from the fits of C (or equivalently $P^{3\gamma}$) and normalized to ν degrees of freedom, is shown in Fig. 7 for the three sample orientations as a function of Δn , the number of electrons moved from the majority- to the minority-spin band.

For large numbers of degrees of freedom ν the quantity $S = (2\chi^2)^{1/2} - (2\nu - 1)^{1/2}$ is normally distributed around zero with unit variance. Hence, it follows that the minimum of χ^2/ν should be slightly less than 1. The values of Δn for which the three curves in Fig. 7 reach their minimum vary from -0.002 for the $\langle 100 \rangle$ curve to -0.023 for $\langle 111 \rangle$. The minimum in the latter curve is very shallow and has a value significantly above 1. Obviously the model is not good for this orientation, and consequently little weight will be given to this orientation. The fit for the $\langle 100 \rangle$ data, although yielding a minimum of 1.30 for χ^2/ν , is particularly sensitive to the transfer of electrons. This sensitivity is due to the fact that the minority-spin Fermi-surface pockets which arise as a re-

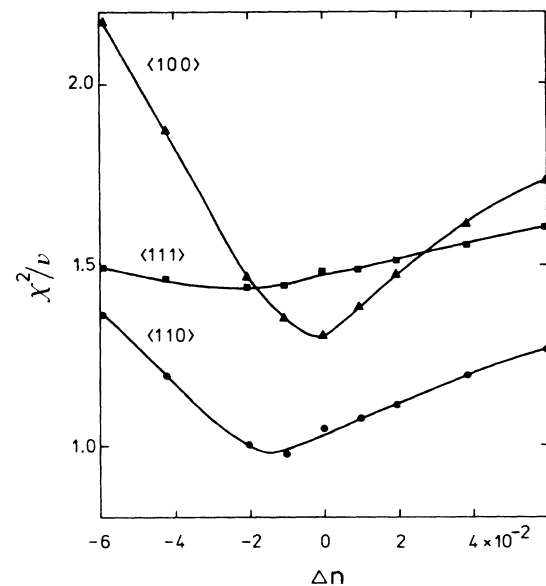


FIG. 7. Normalized χ^2 as a function of the number of electrons Δn transported from the majority- to the minority-spin electron population (and vice versa), obtained from a least-squares fit of computed LCW-folded 2D-ACAR distributions to the experimental ones.

sult of electron transfer (hole pockets around Γ or electron pockets around X) line up most favorably in a $\langle 100 \rangle$ integration. The $\langle 110 \rangle$ fit, finally, gives a minimum slightly below 1 and is moderately sensitive to the electron transfer.

Subsequently, we have relaxed the assumption of sample stoichiometry. In Fig. 8(a)–8(c) the occupation n_+ of the majority-spin band has been varied while n_- , the number of minority-spin electrons, was kept constant at values around 9.00, the number corresponding to a full minority-spin band. Interestingly, for the $\langle 100 \rangle$ integration χ^2/ν reaches a (shallow) minimum at 13.08 (9.00) $+(-)$ electrons, while the chemical constitution corresponds to an excess of 0.07 electrons/f.u. This agreement may be fortuitous since for the $\langle 110 \rangle$ orientation of the same sample the minimum is found at 13.00 (8.99) $+(-)$ electrons. As described in Sec. III, in between the $p_x = \langle 110 \rangle$ and $\langle 100 \rangle$ measurements the sample was cut in a different shape, so the different positions of the mini-

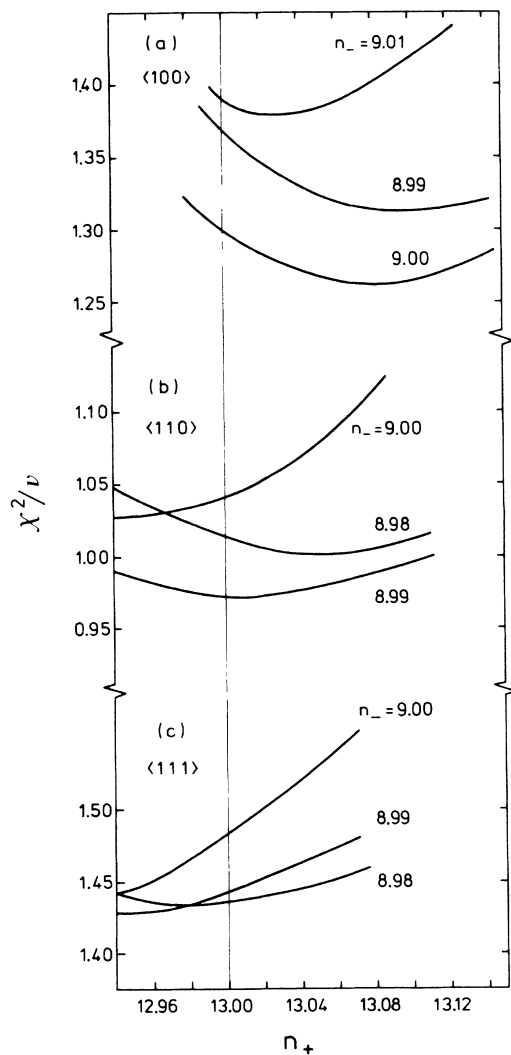


FIG. 8. Normalized χ^2 as a function of the number n_+ of majority-spin electrons for various n_- around 9.00 minority electrons per formula unit. Integration direction along (a), $\langle 100 \rangle$; (b), $\langle 110 \rangle$; (c), $\langle 111 \rangle$.

ma in χ^2/ν may reflect small inhomogeneities in the chemical composition of the sample. Subsequently, the number of majority-spin electrons was kept fixed at 13.00, while the number of minority-spin electrons was varied between 8.94 and 9.06. The resulting values of χ^2/ν are shown in Fig. 9. The positions of the minima in χ^2/ν , vary from $n_- = 8.999$ for $\langle 100 \rangle$ to 8.99 for $\langle 110 \rangle$ and 8.98 for $\langle 111 \rangle$. The dashed curve shows χ^2/ν for $\langle 100 \rangle$ if $n_+ = 13.08$. Its minimum is located at 8.997 and is somewhat lower than that of the corresponding solid curve.

An estimate of the standard deviation in these numbers is obtained by finding those values of n_- for which χ^2/ν has increased by an amount $(2/\nu)^{1/2}$ with respect to its minimum value. A weighted average over the three symmetry directions finally yields $n_- = 8.995 \pm 0.012 \pm 0.020$ electrons/f.u. Thus, we find no significant deviation from the half-metallic state.

The resolution in the present experiment of structures in reciprocal space corresponding to approximately 0.02 electrons/f.u. is made possible by the use of least-squares fits between theory and experiment. Direct observation of these structures is beyond our capability at the present statistical accuracy. Fermi-surface pockets of this volume would have a diameter of somewhat less than 2 mrad, which is about three times the width of our angular resolution (excluding smoothing), and hence in principle would be large enough to be detected. However, the momentum dependence of the overlap integral prevents observation of the hole pockets around Γ in the first Brillouin zone. Only in the second Brillouin zones, in the neighborhood of the points equivalent to $\mathbf{p} = (2\pi/a)(1, 1, 1)$, the momentum density is appreciable (~ 0.14).

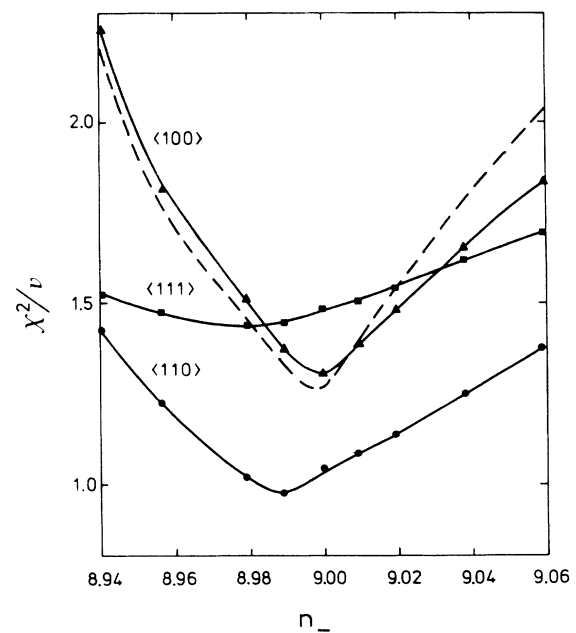


FIG. 9. Normalized χ^2 as a function of the number n_- of minority spin electrons for $n_+ = 13.00$ (solid curves) and $n_+ = 13.08$ (dashed curve for $\langle 100 \rangle$ orientation).

States in the electron pockets around X contribute modestly at points $(2\pi/a)(1,0,0)$ and $(2\pi/a)(1,1,0)$ (in both cases ~ 0.05).

The relatively high minimum values of χ^2/ν for the $\langle 100 \rangle$ and $\langle 111 \rangle$ orientations imply systematic errors in the model used. An important source of error will be the neglect of enhancement in the calculated momentum density and LCW-folded distributions. In view of the uncertainties besetting the inclusion of enhancement in momentum density calculations no attempt has been made to remedy this point. Other (probably smaller) sources of error may be the simplifying assumptions in KKR band theory such as the muffin-tin form of the potential.

In summary, the 2D-ACAR method has been used to measure the spin-dependent momentum density in the ferromagnetic $C1_b$ Heusler compound NiMnSb. The measurements confirm the theoretically predicted half-metallic character of the band structure to within an accuracy of approximately ${}_{-0.02}^{+0.01}$ electrons/f.u.

ACKNOWLEDGMENTS

The authors wish to thank A. J. Riemersma for the spark erosion of the sample, Dr. J. de Vries for the lifetime measurements, and A. C. Letsch and G. Hamburg for the microprobe measurements. It is a pleasure to acknowledge the excellent technical assistance over the years of G. J. Langedijk. This work is part of the research program of the Stichting Fundamenteel Onderzoek der Materie (Foundation for Fundamental Research on Matter) and was made possible by financial support from the Nederlandse Organisatie voor Wetenschappelijk Onderzoek (Netherlands Organization for the Advancement of Research).

APPENDIX A

The total annihilation rate for slow positrons with spin parallel (antiparallel) to the magnetization is given by¹⁸

$$\lambda_{+(-)} = (\frac{1}{2}\lambda_s + \frac{1}{2}\lambda_t)\rho_{+(-)} + \lambda_t\rho_{- (+)}, \quad (\text{A1})$$

where λ_s and λ_t are the 2γ and 3γ annihilation rates per electron per unit volume and $\rho_\sigma \equiv \int \rho_\sigma(\mathbf{p})d\mathbf{p}$ are integrals of the computed majority-spin (+) and minority-spin (-) momentum densities. 2D-ACAR measurements with magnetization parallel (\uparrow) or antiparallel (\downarrow) to the average polarization P of the positron beam yield¹⁸

$$N_{\uparrow(\downarrow)}(p_y, p_z) = \frac{1}{4}\lambda_s [(1 \pm P)\lambda_+^{-1}\rho_+(p_y, p_z) + (1 \mp P)\lambda_-^{-1}\rho_-(p_y, p_z)], \quad (\text{A2})$$

where the upper (lower) sign corresponds to a parallel (antiparallel) magnetization. Insertion of Eq. (A1) into (A2) gives, with $\beta \equiv \lambda_t/\lambda_s = 1/1,114$:

$$N_{\uparrow(\downarrow)}(p_y, p_z) = \frac{1}{2} \left[\frac{(1 \pm P)\rho_+(p_y, p_z)}{\rho_+[1 + \beta(\rho_+ + 2\rho_-)/\rho_+]} + \frac{(1 \mp P)\rho_-(p_y, p_z)}{\rho_-[1 + \beta(\rho_- + 2\rho_+)/\rho_-]} \right]. \quad (\text{A3})$$

This can be simplified if, following Berko,³⁴ a quantity P_e , the effective total electron polarization as seen by the positron, is introduced. Then

$$\begin{aligned} \rho_+ &= \frac{1}{2}(1 - P_e)\rho^{\text{tot}}, \\ \rho_- &= \frac{1}{2}(1 + P_e)\rho^{\text{tot}}, \end{aligned} \quad (\text{A4})$$

where ρ^{tot} denotes the total density of electrons in momentum space. If the positron wave function were a constant, P_e would be negative in a ferromagnetic material as the majority of the electrons have their spin antiparallel to the applied magnetic field. With Eqs. (A4)

$$(\rho_+ + 2\rho_-)/\rho_+ = (3 + P_e)/(1 - P_e), \quad (\text{A5})$$

$$(\rho_- + 2\rho_+)/\rho_- = (3 - P_e)/(1 + P_e),$$

and hence it follows that to first order in β

$$\begin{aligned} \Delta N(p_y, p_z) &= N_{\uparrow}(p_y, p_z) - N_{\downarrow}(p_y, p_z) \\ &= (1 - 3\beta)P \left[\frac{\rho_+(p_y, p_z)}{\rho_+}(1 - 4\beta P_e) - \frac{\rho_-(p_y, p_z)}{\rho_-}(1 + 4\beta P_e) \right], \end{aligned} \quad (\text{A6})$$

with a similar expression for $\Sigma N(p_y, p_z)$.

The prefactor $1 - 3\beta$ has the character of a common scale factor and may therefore be dropped. The factors $1 \pm 4\beta P_e$ equal unity within ~ 1 part in 10^4 . This may be seen by integrating Eq. (A3) with respect to p_y and p_z , using Eqs. (A5). The result is

$$\begin{aligned} N_{\uparrow(\downarrow)}^2 &\equiv \int \int N_{\uparrow(\downarrow)}(p_y, p_z) dp_y dp_z \\ &\approx 1 - \beta \frac{3 + P_e^2}{1 - P_e^2} \mp \beta \frac{4PP_e}{1 - P_e^2}. \end{aligned} \quad (\text{A7})$$

The second and third term are due to 3γ annihilation. Since

$$N_{\uparrow(\downarrow)}^2 + N_{\downarrow(\uparrow)}^2 = 1, \quad (\text{A8})$$

application of Eq. (A7) yields for the three-photon difference effect $P^{3\gamma}$,

$$P^{3\gamma} = \frac{N_{\uparrow}^2 - N_{\downarrow}^2}{N_{\uparrow}^2 + N_{\downarrow}^2} \approx \frac{4PP_e}{3 + P_e^2}, \quad (\text{A9})$$

where $N_{\uparrow(\downarrow)}^2$ is the field-dependent rate of 3γ events. The second line of Eq. (A9) holds if the counters integrate over the full solid angle. When the counters are situated in one plane the final expressions for $P^{3\gamma}$ must be multiplied^{18,35} by a factor $\frac{3}{4}$. Berko and Mills¹⁸ have measured $P^{3\gamma}$ in the latter geometry and have found values ranging between -0.009 and $+0.001$. With $P \approx 0.3$ this results in $|P_e| \approx 0.03$, and hence the factors $1 \pm 4\beta P_e$ may be omitted from Eq. (A6), proving the validity of Eqs. (2) and (3).

The constant C defined in Eq. (5) is directly related to $P^{3\gamma}$. With Eqs. (A4) and (A9) one obtains

$$C = PP_e \approx P^{3\gamma} \quad (\text{A10})$$

with $P^{3\gamma}$ measured in the planar geometry.

*Present address: Philips Research Laboratories, 5600 JA Eindhoven, The Netherlands.

- ¹R. A. De Groot, F. M. Mueller, P. G. Van Engen, and K. H. J. Buschow, *Phys. Rev. Lett.* **50**, 2024 (1983).
- ²R. A. De Groot, F. M. Mueller, P. G. Van Engen, and K. H. J. Buschow, *J. Appl. Phys.* **55**, 2151 (1984).
- ³J. Kübler, *Physica (Utrecht)* **127B**, 257 (1984).
- ⁴A. Yanase and K. Siratori, *J. Phys. Soc. Jpn.* **53**, 312 (1984).
- ⁵K. Schwarz, *J. Phys. F* **16**, L211 (1986).
- ⁶R. C. Albers, A. M. Boring, G. H. O. Daalderop, and F. M. Mueller, *Phys. Rev. B* **36**, 3661 (1987).
- ⁷P. G. Van Engen, Ph.D. thesis, Technological University Delft, 1983.
- ⁸P. A. M. Van der Heide, W. Baelde, R. A. De Groot, A. R. De Vroomen, P. G. Van Engen, and K. H. J. Buschow, *J. Phys. F* **15**, L75 (1985).
- ⁹G. L. Bona, F. Meier, M. Taborelli, E. Bucher, and P. H. Schmidt, *Solid State Commun.* **56**, 391 (1985).
- ¹⁰E. Kisker, C. Carbone, C. F. Flipse, and E. F. Wasserman, *J. Magn. Magn. Mater.* **70**, 21 (1987).
- ¹¹M. J. Otto, H. Feil, R. A. M. Van Woerden, J. Wijngaard, P. J. Van der Valk, C. F. Van Bruggen, and C. Haas, *J. Magn. Magn. Mater.* **70**, 33 (1987).
- ¹²R. B. Helmholtz, R. A. De Groot, F. M. Mueller, P. G. Van Engen, and K. H. J. Buschow, *J. Magn. Magn. Mater.* **43**, 249 (1984).
- ¹³P. G. Van Engen, K. H. J. Buschow, R. Jongebreur, and M. Erman, *Appl. Phys. Lett.* **42**, 202 (1983).
- ¹⁴K. P. Kämper, W. Schmitt, G. Güntherodt, R. J. Gambino, and R. Ruf, *Phys. Rev. Lett.* **59**, 2788 (1987).
- ¹⁵N. Bykovetz, W. N. Herman, T. Yuen, Chan-Soo Jee, C. L. Lin, and J. E. Crow, *J. Appl. Phys.* **63**, 4127 (1988).
- ¹⁶W. Brandt and R. Paulin, *Phys. Rev. B* **15**, 2511 (1977).
- ¹⁷K. E. H. M. Hanssen and P. E. Mijnen, *Phys. Rev. B* **34**, 5009 (1986).
- ¹⁸S. Berko and A. P. Mills, *J. Phys. (Paris) Colloq.* **32**, C1-287 (1971).
- ¹⁹P. Zwart, L. P. L. M. Rabou, G. J. Langedijk, A. P. Jeavons, A. P. Kaan, H. J. M. Akkerman, and P. E. Mijnen, in *Positron Annihilation*, edited by P. C. Jain, R. M. Singru, and K. P. Gopinathan (World Scientific, Singapore, 1985), p. 297.
- ²⁰L. P. L. M. Rabou, Ph.D. thesis, University of Amsterdam, 1983 (Netherlands Energy Research Foundation ECN Report No. ECN-129, Petten, 1983).
- ²¹K. E. H. M. Hanssen, Ph.D. thesis, University of Amsterdam, 1988 (Netherlands Energy Research Foundation ECN Report No. ECN-209, Petten, 1988); cf. Appendix 6b [please note that in both these publications the denominator in Eq. (6.3) and in the corresponding equation for X in the Appendix should read $\rho_- - \rho_+$].
- ²²D. G. Lock, V. H. C. Crisp, and R. N. West, *J. Phys. F* **3**, 561 (1973).
- ²³S. Berko, in *Positron Solid-State Physics*, edited by W. Brandt and A. Dupasquier (North-Holland, Amsterdam, 1983), p. 64.
- ²⁴E. Bonderup, J. U. Andersen, and D. N. Lowy, *Phys. Rev. B* **20**, 883 (1979).
- ²⁵L. P. L. M. Rabou, P. Zwart, G. J. Langedijk, and P. E. Mijnen (Netherlands Energy Research Foundation ECN, Report No. ECN-211, Petten, 1988) (unpublished).
- ²⁶H. J. Mikeska, *Z. Phys.* **232**, 159 (1973).
- ²⁷M. A. Shulman, G. M. Beardsley, and S. Berko, *Appl. Phys.* **5**, 367 (1975).
- ²⁸A. T. Stewart, J. B. Shand, and S. M. Kim, *Proc. Phys. Soc. London* **88**, 1001 (1966).
- ²⁹S. M. Kim and A. T. Stewart, *Phys. Rev. B* **11**, 2490 (1975).
- ³⁰In view of the temporary availability of an ETA10-P232 supercomputer the KKR calculations of Ref. 17 have been repeated to check their convergence. The same crystal potential was used as before with muffin-tin spheres of uniform size. The new computations were done on a finer mesh of 505 k points in the irreducible $\frac{1}{48}$ th of the Brillouin zone and included terms up to $l_{\max} = 3$. The momentum density was computed for $\sim 191\,000$ \mathbf{p} vectors in $\frac{1}{48}$ th of a sphere with radius 4.5 a.u. No significant differences were found between the two computations.
- ³¹P. E. Mijnen and L. P. L. M. Rabou, *J. Phys. F* **16**, 483 (1986).
- ³²P. E. Mijnen and A. Bansil, *J. Phys. Condens. Matter* **2**, 911 (1990).
- ³³K. H. J. Buschow, P. G. Van Engen, and R. Jongebreur, *J. Magn. Magn. Mater.* **38**, 1 (1983).
- ³⁴S. Berko, in *Positron Annihilation*, edited by A. T. Stewart and L. O. Roellig (Academic, New York, 1967), p. 61.
- ³⁵P. E. Mijnen, *Physica (Utrecht)* **63**, 248 (1973).